Scripta Materialia 285 (2026) 117525

Contents lists available at ScienceDirect

Scripta Materialia

journal homepage: www.journals.elsevier.com/scripta-materialia

Role of material parameters in tribological stress field models

Antje Dollmann [a,b,*], Alexander Dyck [c], Claudius Klein [c], Alexander Kauffmann [a], Thomas Böhlke [c], Christian Greiner [a,b]

[a] Institute for Applied Materials (IAM), Karlsruhe Institute of Technology (KIT), Kaiserstraße 12, 76131 Karlsruhe, Germany
[b] IAM-ZM MicroTribology Center (μTC), Straße am Forum 5, 76131 Karlsruhe, Germany
[c] Continuum Mechanics, Institute of Engineering Mechanics (ITM), Karlsruhe Institute of Technology (KIT), Kaiserstraße 12, 76131 Karlsruhe, Germany

ARTICLE INFO

Keywords:
Tribology
Stress field
Twins
Crystal plasticity

ABSTRACT

Microstructural evolution in metallic materials feedbacks with the loading conditions and the lifetime of engineering components. Tribological loading causes a complex, position-dependent, moving stress field. A systematic study is presented on the influence of the complexity of the implemented material model on the calculated stress field. For validation, results of tribological experiments on single crystals with the activation of deformation twinning are used. The calculated resolved shear stresses have to be highest on the experimentally identified twin systems. The combination of modelling and experiment shows the necessity of considering plasticity. The widely used Hamilton stress field for tribological loading is limited and based on purely elastic assumptions. The quality of the stress field is found to be sensitive to the yield strength, work hardening and plastic anisotropy. These parameters have to be carefully chosen in order to predict how a metallic material deforms due to a sliding load.

Tribological contacts are ubiquitous. Technical applications without any relation to tribology are quasi non-existent. Unfortunately, tribological phenomena are complex and have numerous influencing parameters. To make matters worse, tribological properties are not material constants, but system properties. Among the many parameters, we here focus on the subsurface deformation layer developing in materials with plastic behaviour. The concept of friction feedback loop states that the friction coefficient influences the stress field resulting in microstructural evolution which itself feedbacks with the friction coefficient [1,2]. While this demonstrates the complexity and interwovenness of tribological processes, it also means that a classical microstructure-properties relation exists. However, the microstructure undergoes drastic changes as the tribological load is applied. Such microstructural evolution is not only known to change friction forces, but also to initiate cracks resulting in wear particle formation and failure of engineering components [3–5].

In general, the microstructural evolution in metallic materials is caused by plastic deformation mechanisms, i.e., dislocation slip and deformation twinning. These fundamental mechanisms are activated by (resolved) shear stresses (RSS) reaching a material-specific, critical value τ_c.

Tribological systems exhibit inhomogeneous, multi-axial, position-dependent stresses, which are moving with the counter body. Thus, analysing the activation and evolution of deformation mechanisms requires an adequate description of the stress field.

As this matter has been recognized for several decades, several approaches exist in the literature. Therefore, the most common stress field models are briefly summarized and arranged in order of their complexity. Literature does not address the limits or the range of usability of these models. This challenging task is desperately needed.

The easisiest approach is to only consider singular components of the stress tensor. Researchers have relied on a pure shear stress or a pure normal stress in normal or sliding direction, respectively [6–8]. This highly simplifies the calculation of active slip systems while neglecting the lateral stress distribution, multiaxiality and plastic material behaviour completely.

The next complexity level is a multiaxial analytical, static solution. Hamilton's approach superimposes a Hertzian contact with a shear stress proportional to the friction coefficient assuming isotropic, linear-elastic material behaviour [9]. Despite its limitations, Hamilton's model is often used in literature to rationalize microstructural evolution in metallic materials [10–15]. It was also employed to investigate dislocation-mediated plastic deformation using discrete dislocation dynamics simulations [16]. Nevertheless, prior work has demonstrated

* Corresponding author at: Karlsruhe Institute of Technology, Germany.
E-mail address: antje.dollmann@kit.edu (A. Dollmann).

https://doi.org/10.1016/j.scriptamat.2026.117525
Received 28 April 2026; Received in revised form 15 July 2026; Accepted 5 August 2026
Available online 6 August 2026

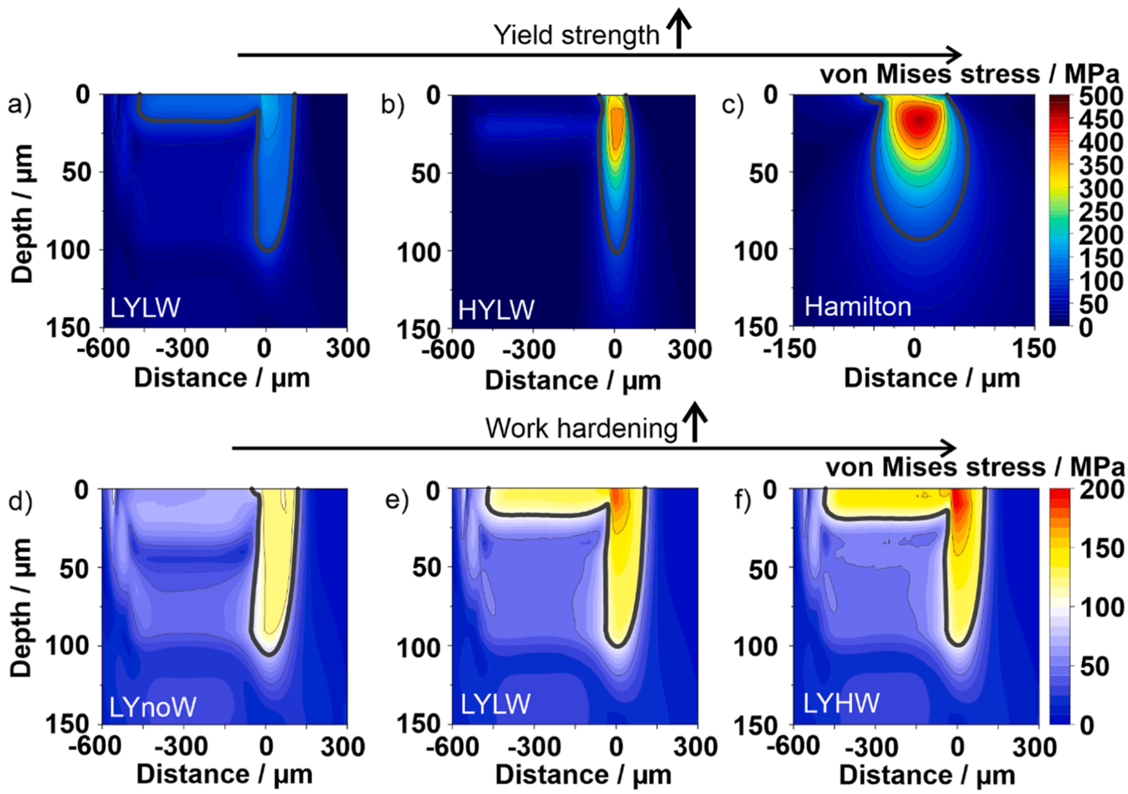

Fig. 1. Von Mises stresses for the isotropic material models. The first row shows the influence of increasing yield strength from left to right. The von Mises stress using the material model LYLW is shown in a), HYLW in b) and Hamilton in c). Increasing work hardening is investigated in the second row from left to right. Hereby, the yield strength was kept constant. The material model LYnoW is investigated in d), LYLW in e) and LYHW in f). Different color-coding was used for a)-c) and d)-f) to show the different scaling. The abbreviations HY and LY stand for high yield strength and low yield strength, respectively. noW, LW and HW indicate the degree of work hardening: no work hardening, low work hardening and high work hardening. The spherical counter body starts sliding at the distance of −500 µm except for the Hamilton model, where the indenter remains at 0 µm. The current loading position is at 0 µm. The friction coefficient is 0.2.

limitations [17].

Due to plastic deformation, models assuming purely linear-elastic behaviour largely overestimate the stresses acting in the contact and their penetration depth as both are reduced upon plastic flow. Plasticity effects were studied by various simulation methods on different length scales. These non-static frameworks have the advantage of a moving counter body, capturing the history of the contact. For example, a correlation between the deformation mechanisms and the stress field was investigated by molecular dynamic simulations (MD) [18].

Those are restricted to a few million atoms and high strain rates favouring stacking fault formation and deformation twinning, based on computational limits [19].

For larger sample sizes, finite element simulations (FEM) were used. Literature using classical FEM calculating the stress field is limited [20, 21]. Recent studies used crystal plasticity FEM simulations (CP-FEM) to simulate the materials plastic response under tribological loading [22–25]. Experiments and simulations were compared regarding wear track depth, material pile-up and crystal rotation [22–24,26]. Reasonable agreement between simulation and experiment was reported, predicting crystallographic rotations concerning their sign. However, the lateral extent of the subsurface affected by plasticity were off.

For the above as well as for future simulations, there is one constant challenge: How to validate the modelled stress field predictions experimentally. Our approach follows two prongs. First, a useful stress field model has to be able to accurately predict the resolved shear stresses on twin systems. Second, we investigate how different material parameters change the stress field calculated with FEM. These prongs are combined and the resolved shear stresses on all possible twin systems are calculated. This has to agree with experimentally identified twin systems, thereby validating the stress fields. The purpose of the manuscript is to systematically investigate the effect of material properties on the stress field.

First, material parameters are tested and their influence on the stress field evaluated. The material parameters considered are yield strength, work hardening behaviour and elastic and plastic anisotropy. Details concerning the FE simulations can be found in the Supplementary Information (SI). The chosen material parameters correspond to experimentally determined values for CoCrFeMnNi, as this alloy was investigated for reference experiments.

Isotropic material models with different yield strength were investigated: 125 MPa labelled as LY (low yield strength) and 360 MPa labelled as HY (high yield strength) [27]. In addition, three different work hardening behaviours are considered: no work hardening (noW), low work hardening (LW) and high work hardening (HW) [28]. The elastic and plastic anisotropy was investigated employing crystal plasticity (CP) model (labelled CP-FEM) with a τ_c for dislocation motion of 43 MPa [29]. No work hardening was considering based on the challenges posed by calibrating these values, as for example shown in reference [30]. Performing such a calibration, especially for our complex stress state with deformation twinning, is outside the scope of the current manuscript. For all models, a friction coefficient of 0.2 is used. This choice is based on experimental data for the first stroke [17].

The material parameters effects are visible in the von Mises stress plots in Fig. 1. For the sake of clarity, only the isotropic materials models are shown and the anisotropic in Figure S6 (SI).

Comparing the panels shown in Fig. 1, one notices one communality: The lowest z-position of the 100 MPa isoline always is at a depth of around 100 µm. This suggests that the depth of the stress field is marginally influenced by the material model. Strikingly, the depth of the stress field is orders of magnitude deeper than the observed

Table 1
Summary of the occurrence of deformation twins in single crystalline CoCrFeMnNi under tribological loading. The determined twin systems are mentioned. The corresponding STEM and HR-TEM images can be found in [17].

	ND[00$\bar{1}$]/ SD[$\bar{1}$10]	ND[0$\bar{1}\bar{1}$]/ SD[100]	ND[0$\bar{1}\bar{1}$]/ SD[0$\bar{1}$1]	ND[0$\bar{1}\bar{1}$]/ SD[$\bar{2}\bar{1}$1]	ND[00$\bar{1}$]/ SD[100]
Twins	✓	✓	×	×	×
Twin system	($\bar{1}$11)[$\bar{1}$1$\bar{2}$]	($\bar{1}\bar{1}\bar{1}$)[2$\bar{1}\bar{1}$]	-	-	-

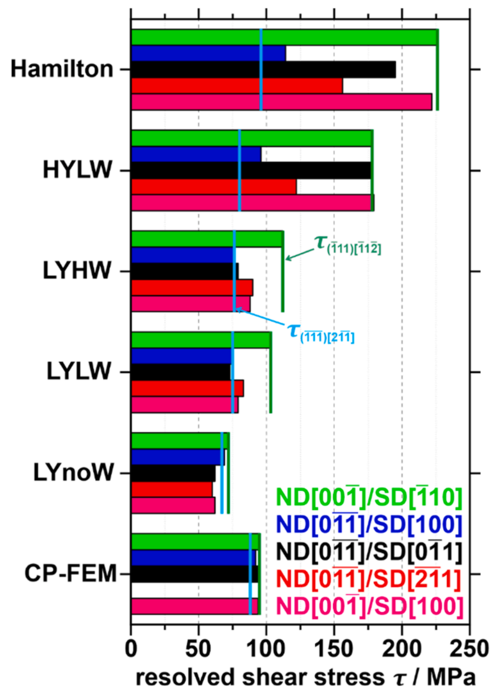

Fig. 2. Maximum resolved shear stresses for the experimentally investigated crystal orientations and six investigated material models: Hamilton, HYLW, LYHW, LYLW, LYnoW and CP-FEM. The red bar for CP-FEM is missing based on lacking crystallographic symmetry (see SI). The experimentally identified twin system for the crystal orientation ND[00$\bar{1}$]/SD[$\bar{1}$10] is ($\bar{1}$11)[$\bar{1}$1$\bar{2}$]. ($\bar{1}\bar{1}\bar{1}$)[2$\bar{1}\bar{1}$] is the experimentally identified twin system for the crystal orientation ND[0$\bar{1}\bar{1}$]/SD[100]. The resolved shear stresses on these two twin systems ($\tau_{(\bar{1}11)[\bar{1}1\bar{2}]}$ and $\tau_{(\bar{1}\bar{1}\bar{1})[2\bar{1}\bar{1}]}$) are marked by the green and blue lines for each material model.

microstructural evolution [17].

This significant discrepancy between simulation and experiment might be due to the assumption of a flat, non-rough surface, or the fact that not all dislocation activity was or possibly can be experimentally detected. Simulations have shown a deeper extend of statistically stored dislocations below the surface than for geometrically necessary ones [25]. The first ones cannot be measured with our method. Significant deviations between the different material models are seen in the position and the value of the maximum von Mises stress. The Hamilton model yields a maximum of 452 MPa in a depth of 17 µm. HYLW results in a maximum of 362 MPa at a depth of 15 µm. In contrast, considering a lower yield strength (LYLW) results in a maximum of 181 MPa at the surface. When investigating different work hardening behaviour for the low yield strength case, the following is observed: high work hardening results into a maximum of 197 MPa in a depth of 5 µm, whereas the maximum for no work hardening is 125 MPa at the surface. A maximum von Mises stress at the surface agrees with the experimental data as the most pronounced microstructural evolution is observed in the near surface region. In the literature, a multiaxiality factor was introduced to describe the discrepancy between the von Mises stress maximum according to the Hamilton model and the pronounced microstructural changes directly beneath the surface [12]. While this approach was successful, it seems likely that plasticity must be considered rather than tweaking a purely elastic stress field.

As stress field models should be capable of successfully predicting experimental reality, we approach such validation by calculating the resolved shear stresses for experimentally observed deformation twin systems. Deformation twins are chosen as probes as they are indicative of the plane and direction they were formed on and can be analyzed by ex-situ microstructural investigations. This contrasts with dislocation motion where cross-slip, annihilation and bidirectionality leaves ambiguity. We have earlier described single trace tribological experiments on face-centred cubic CoCrFeMnNi single crystals with defined normal (ND) and sliding directions (SD) [17]. In two out of five crystallographic orientations investigated, deformation twins were observed within the deformation layer. These results are summarized in Table 1.

The results for the maximum resolved shear stresses as calculated from the five stress fields models - Hamilton, HYLW, LYnoW, LYLW, LYLW, LYHW and CP-FEM – are represented in Fig. 2. The Hamilton model is given as a reference and as it is the most commonly taken in literature, albeit these results were already presented in [17]. In this plot, each bar represents the maximum RSS among all twin systems for one specific crystallographic orientation and material model, without providing information about the specific twin system. The RSS values on the experimentally identified twin systems are represented by the green and blue lines for the RSS on ($\bar{1}$11)[$\bar{1}$1$\bar{2}$] for ND[00$\bar{1}$]/SD[$\bar{1}$10] ($\tau_{(\bar{1}11)[\bar{1}1\bar{2}]}$) and on ($\bar{1}\bar{1}\bar{1}$)[2$\bar{1}\bar{1}$] for ND[0$\bar{1}\bar{1}$]/SD[100] ($\tau_{(\bar{1}\bar{1}\bar{1})[2\bar{1}\bar{1}]}$), respectively.

First, the results based on the Hamilton model are summarized. The focus hereby is on the experimentally identified twin systems. The twin system ($\bar{1}$11)[$\bar{1}$1$\bar{2}$] for ND[00$\bar{1}$]/SD[$\bar{1}$10] exhibits the highest overall RSS. In contrast, $\tau_{(\bar{1}\bar{1}\bar{1})[2\bar{1}\bar{1}]}$ for ND[0$\bar{1}\bar{1}$]/SD[100] is not the highest RSS for this orientation and it is lower than all the other maximum RSS of the investigated crystallographic orientations. Although, the Hamilton model shows the correct result for ND[00$\bar{1}$]/SD[$\bar{1}$10], it does not provide the correct results for ND[0$\bar{1}\bar{1}$]/SD[100], as other twin systems, which were experimentally not activated, have higher RSS. Therefore, the Hamilton model is invalid for the given tribological setting when assuming a single, material specific critical stress τ_c.

The effect of yield strength is investigated considering the material models: Hamilton, HYLW and LYLW. As expected, a decrease in yield strength results in lower resolved shear stresses, which is dependent on crystallographic orientation. Comparing Hamilton and LYLW, the highest decrease in RSS of 60 % is calculated for ND[00$\bar{1}$]/SD[100] and the smallest of 22 % for ND[00$\bar{1}$]/SD[$\bar{1}$10]. Considering different work hardening behaviors, while keeping LY constant, show qualitatively similar effects as the yield strength variation. Comparing noW and HW results into the greatest difference of 40 MPa (35%) for ND[00$\bar{1}$]/SD[$\bar{1}$10] and the lowest of 7 MPa (10%) for ND[0$\bar{1}\bar{1}$]/SD[100]. As demonstrated in Ref., [17], the position of the resolved shear stress maximum with respect to the indenter position varies with the crystallographic orientation and selected twin system. This position variation has an influence on the differences in resolved shear stress.

For investigating the effect of elastic and plastic anisotropy, no work hardening was considered in CP-FEM to ensure comparability with LYnoW which avoids influencing effects besides anisotropy. Additionally, the critical RSS for dislocation motion within the CP-FEM framework is equal to LY divided by the Taylor factor. Only four out of the five crystallographic orientations were simulated, based on modelling limitations. In comparison to LYnoW, the RSS using CP-FEM is increased by at least 31 %. The CP-FEM model could not reflect the experiments as crystallographic orientations without experimentally verified twinning have higher RSS than $\tau_{(\bar{1}\bar{1}\bar{1})[2\bar{1}\bar{1}]}$ and furthermore, $\tau_{(\bar{1}\bar{1}\bar{1})[2\bar{1}\bar{1}]}$ is not the highest value within ND[0$\bar{1}\bar{1}$]/SD[100]. Incorporating work hardening to the CP-FEM model is the next parameter to be considered. However, choosing the proper microscopic strain hardening model and

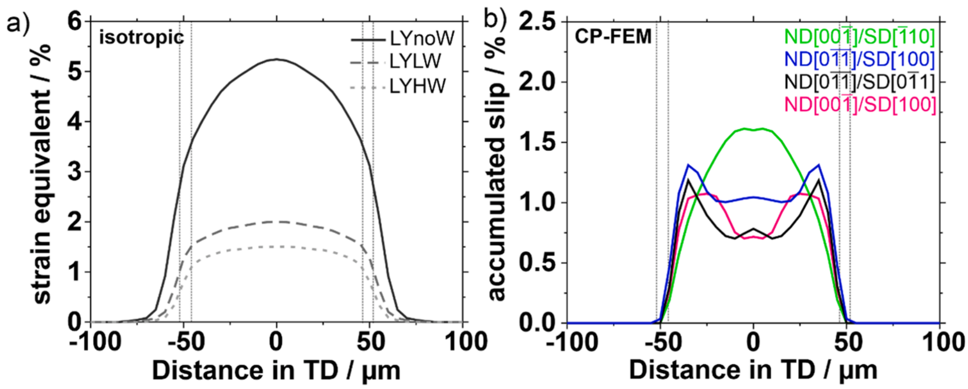

Fig. 3. Equivalent strain/accumulated slip on the surface perpendicular to the sliding direction (=transverse direction (TD)). The range of the wear track width from the experimental data is represented by the dotted vertical lines. a) influence of the investigated work hardening behaviours with low yield strength (125 MPa); b) influence of the crystal orientation dependency on the accumulated slip (CP-FEM model).

parameters, them being themselves compatible with classical FEM models, is a challenge. Furthermore, the stress release and hardening by deformation twinning is then still not mapped and will impact the results. As shown in Ref., [30], even with a symmetric crystallographic orientation and simple indentation, reproducing the experiment using CP-FEM is challenging. Here, the isotropic material models LYnoW and LYLW show the best results with the given settings, specifically considering the substantially increased complexity of CP-FEM.

Finally, the critical shear stress for twinning in CoCrFeMnNi at RT has to be discussed. The lowest experimentally measured value is 110 MPa [31]. $\tau_{(\overline{111})[2\overline{11}]}$ calculated with all stress field models is lower than 110 MPa. The difference could arise through a stress concentration not covered by the simulation, or a possibly limited comparability between twin formation under uniaxial and multiaxial stress.

Besides the RSS approach, the experimentally obtained wear track width is compared to the widths of the plastic strain on the surface in the transversal direction in the simulations (Fig. 3). The wear track width is easily accessible and only requires optical microscopy. Hamilton and HYLW are missing as these did not result in any plastic strain or plastic strain on the surface (Hamilton is purely elastic; the plastic strain for HYLW is given in Figure S7). Work hardening changes mainly the values of the maximum plastic strain and not the width as shown in Fig. 3a. The full width half maximum (FWHM) lies for all three material models calculated with LY between 100 and 110 µm (finite element size of 5 µm). The mean experimental wear track widths vary between 97 and 104 µm, therefore, the simulations with LY are closest to the experiment. A perfect match is achieved with the width of the accumulated slip for CP-FEM in Fig. 3b From this perspective, CP-FEM is in best agreement with the measured wear track width. The approach of comparing the experimental wear track width with the extent of equivalent strain or accumulated slip yielded results consistent with the RSS discussion above. It did, however, not allow to further discard material models.

In summary, six material models were applied to simulate tribological stress fields, five were using the finite element method. The aim was to systematically investigate how the stress field is affected by varying material parameters such as yield strength, work hardening and elastic and plastic anisotropy were considered to investigate their respective effects. Analyzing the von Mises stress distribution shows a decrease in its maximum and shift towards the surface with increasing proportion of plastic deformation showing the inaccuracy of the Hertzian model's prediction of a subsurface stress maximum several micrometers beneath the surface. To analyze which model is most suitable (at minimum effort in model and parameter selection) to predict the microstructural evolution under tribological loading, two different methods were used: i) A comparison between the experimentally measured wear track width and the width of the strain equivalent/accumulated slip within the simulations; ii) if the stress field models predict the formation of the experimentally observed deformation twins. The first method is experimentally faster and excludes stress field models, with no or little plasticity. All other material models agreed with the experimental results. The second method is significantly more time-consuming. At the same time, twins are very reliable probes for the tribological stress field. None of the investigated stress field models were able to perfectly predict the experimentally observed twins. This limitation may be partly due to the use of a simplified FEM set-up. The resolved shear stress decreases with increasing plasticity, as expected. However, the extend of this decrease is dependent on the crystallographic orientation – also for the isotropic material models – and the position of the resolved shear stress maximum with respect to the indenter. Although not perfect, the results clearly show great improvement for calculating resolved shear stresses when using an isotropic material model compared to the classical Hamilton approach.

Declaration of generative AI and AI-assisted technologies in the manuscript preparation process

During the preparation of this work the authors used ChatGPT in order to improve grammar and spelling. After using this tool/service, the authors reviewed and edited the content as needed and take full responsibility for the content of the published article.

CRediT authorship contribution statement

Antje Dollmann: Writing – original draft, Visualization, Methodology, Investigation, Formal analysis, Conceptualization. **Alexander Dyck:** Writing – review & editing, Investigation. **Claudius Klein:** Writing – review & editing, Investigation, Formal analysis. **Alexander Kauffmann:** Writing – review & editing, Supervision, Conceptualization. **Thomas Böhlke:** Writing – review & editing, Supervision, Conceptualization. **Christian Greiner:** Writing – review & editing, Supervision, Conceptualization.

Declaration of competing interest

The authors declare that they have no known competing financial interests or personal relationships that could have appeared to influence the work reported in this paper.

Acknowledgments

C.G thanks the European Research Council (ERC) for funding under Project 771237 and acknowledges funding from the Deutsche Forschungsgemeinschaft DFG under Grant GR 4174/13.

Supplementary materials

Supplementary material associated with this article can be found, in the online version, at doi:10.1016/j.scriptamat.2026.117525.

Data availability

All raw data and code is available from the authors upon request.

References

[1] D.A. Rigney, Transfer, mixing and associated chemical and mechanical processes during the sliding of ductile materials, Wear 245 (2000) 1–9, https://doi.org/10.1016/S0043-1648(00)00460-9.
[2] N. Argibay, M. Chandross, S. Cheng, J.R. Michael, Linking microstructural evolution and macro-scale friction behavior in metals, J. Mater. Sci. 52 (2017) 2780–2799, https://doi.org/10.1007/s10853-016-0569-1.
[3] W.J. Salesky, R.M. Fisher, R.O. Ritchie, G. Thomas, The nature and origin of sliding wear debris from steels, Wear Mater. (1983) 434–445.
[4] N.P. Suh, The delamination theory of wear, Wear 25 (1973) 111–124.
[5] D.A. Rigney, W.A. Glaeser, The significance of near surface microstructure in the wear process, Wear 46 (1978) 241–250, https://doi.org/10.1016/0043-1648(78)90125-4.
[6] A. Dollmann, A. Kauffmann, M. Heilmaier, A. Srinivasan Tirunilai, L.S. Mantha, C. Kübel, S.J. Eder, J. Schneider, C. Greiner, Dislocation-mediated and twinning-induced plasticity of CoCrFeMnNi in varying tribological loading scenarios, J. Mater. Sci. 57 (2022) 17448–17461, https://doi.org/10.1007/s10853-022-07661-3.
[7] D.V. Lychagin, A.V. Filippov, E.A. Kolubaev, O.S. Novitskaia, Y.I. Chumlyakov, A. V. Kolubaev, Dry sliding of Hadfield steel single crystal oriented to deformation by slip and twinning: deformation, wear, and acoustic emission characterization, Tribol. Int. 119 (2018) 1–18, https://doi.org/10.1016/j.triboint.2017.10.027.
[8] W. Cai, P. Bellon, A.J. Beaudoin, Probing the subsurface lattice rotation dynamics in bronze after sliding wear, Scr. Mater. 172 (2019) 6–11, https://doi.org/10.1016/j.scriptamat.2019.07.002.
[9] G.M. Hamilton, Explicit equations for the stresses beneath a sliding spherical contact, Proc. Inst. Mech. Eng. C: J. Mech. Eng. Sci. 197 (1983) 53–59, https://doi.org/10.1243/PIME_PROC_1983_197_076_02.
[10] C. Greiner, Z. Liu, R. Schneider, L. Pastewka, P. Gumbsch, The origin of surface microstructure evolution in sliding friction, Scr. Mater. 153 (2018) 63–67, https://doi.org/10.1016/j.scriptamat.2018.04.048.
[11] T.J. Rupert, C.A. Schuh, Sliding wear of nanocrystalline Ni–W: structural evolution and the apparent breakdown of Archard scaling, Acta Mater. 58 (2010) 4137–4148, https://doi.org/10.1016/j.actamat.2010.04.005.
[12] A. Fischer, Subsurface microstructural alterations during sliding wear of biomedical metals. Modelling and experimental results, Comput. Mater. Sci. 46 (2009) 586–590, https://doi.org/10.1016/j.commatsci.2009.01.016.
[13] F. Liang, X. Xu, P. Wang, Y. Zhang, Z. Han, X. Chen, Microstructural origin of high scratch resistance in a gradient nanograined 316L stainless steel, Scr. Mater. 220 (2022) 114895, https://doi.org/10.1016/j.scriptamat.2022.114895.
[14] X. Chen, Z. Han, K. Lu, Friction and wear reduction in copper with a gradient nano-grained surface layer, ACS. Appl. Mater. Interfaces. 10 (2018) 13829–13838, https://doi.org/10.1021/acsami.8b01205.
[15] S.V. Prasad, J.R. Michael, C.C. Battaile, B.S. Majumdar, P.G. Kotula, Tribology of single crystal nickel: interplay of crystallography, microstructural evolution, and friction, Wear 458-459 (2020) 203320, https://doi.org/10.1016/j.wear.2020.203320.
[16] J. Gagel, D. Weygand, P. Gumbsch, Discrete Dislocation Dynamics simulations of dislocation transport during sliding, Acta Mater. 156 (2018) 215–227, https://doi.org/10.1016/j.actamat.2018.06.002.
[17] A. Dollmann, C. Kübel, V. Tavakkoli, S.J. Eder, M. Feuerbacher, T. Liening, A. Kauffmann, J. Rau, C. Greiner, Deformation twins as a probe for tribologically induced stress states, Commun. Mater. 5 (2024) 1–10, https://doi.org/10.1038/s43246-023-00442-8.
[18] S.J. Eder, M. Rodríguez Ripoll, U. Cihak-Bayr, D. Dini, C. Gachot, Unraveling and mapping the mechanisms for near-surface microstructure evolution in CuNi alloys under sliding, ACS. Appl. Mater. Interfaces. 12 (2020) 32197–32208, https://doi.org/10.1021/acsami.0c09302.
[19] J.W. Christian, S. Mahajan, Deformation twinning, Prog. Mater. Sci. 39 (1995) 1–157, https://doi.org/10.1016/0079-6425(94)00007-7.
[20] H.A. Padilla, B.L. Boyce, C.C. Battaile, S.V. Prasad, Frictional performance and near-surface evolution of nanocrystalline Ni–Fe as governed by contact stress and sliding velocity, Wear 297 (2013) 860–871, https://doi.org/10.1016/j.wear.2012.10.018.
[21] A. Peela, A. Mikitisin, F. Steinweg, T. Janitzky, A. Schwedt, C. Broeckmann, J. Mayer, Influence of subsurface non-metallic inclusions on rolling contact fatigue behavior in bearing steels - experimental and numerical investigations, Wear 566-567 (2025) 205767, https://doi.org/10.1016/j.wear.2025.205767.
[22] A. Kareer, E. Tarleton, C. Hardie, S.V. Hainsworth, A. Wilkinson, Scratching the surface: elastic rotations beneath nanoscratch and nanoindentation tests, Acta Mater. 200 (2020) 116–126.
[23] J. Zhu, Q. Zhou, Y. Huang, B. Zhou, J. Wang, Surface deformation of single crystalline copper on different nano-scratching paths, J. Mater. Sci. 56 (2021) 10640–10652, https://doi.org/10.1007/s10853-021-05948-5.
[24] Z. Wang, J. Zhang, J. Lu, Effects of crystallographic orientations and grain boundaries on nanoscratching behaviour of unique bi-crystal Cu, Wear 498-499 (2022) 204313, https://doi.org/10.1016/j.wear.2022.204313.
[25] J. Zhu, R. Aghababaei, On the size effect in scratch and wear response of single crystalline copper, Tribol. Int. 186 (2023) 108573, https://doi.org/10.1016/j.triboint.2023.108573.
[26] A. Kareer, E. Demir, E. Tarleton, C. Hardie, Localised stress and strain distribution in sliding, Scr. Mater. 263 (2025) 116662, https://doi.org/10.1016/j.scriptamat.2025.116662.
[27] F. Otto, A. Dlouhỳ, C. Somsen, H. Bei, G. Eggeler, E.P. George, The influences of temperature and microstructure on the tensile properties of a CoCrFeMnNi high-entropy alloy, Acta Mater. 61 (2013) 5743–5755.
[28] G. Laplanche, P. Gadaud, O. Horst, F. Otto, G. Eggeler, E.P. George, Temperature dependencies of the elastic moduli and thermal expansion coefficient of an equiatomic, single-phase CoCrFeMnNi high-entropy alloy, J. Alloys. Compd. 623 (2015) 348–353, https://doi.org/10.1016/j.jallcom.2014.11.061.
[29] M. Kawamura, M. Asakura, N.L. Okamoto, K. Kishida, H. Inui, E.P. George, Plastic deformation of single crystals of the equiatomic Cr−Mn−Fe−Co−Ni high-entropy alloy in tension and compression from 10 K to 1273 K, Acta Mater. 203 (2021) 116454, https://doi.org/10.1016/j.actamat.2020.10.073.
[30] N. Zaafarani, D. Raabe, R.N. Singh, F. Roters, S. Zaefferer, Three-dimensional investigation of the texture and microstructure below a nanoindent in a Cu single crystal using 3D EBSD and crystal plasticity finite element simulations, Acta Mater. 54 (2006) 1863–1876, https://doi.org/10.1016/j.actamat.2005.12.014.
[31] I.V. Kireeva, Y.I. Chumlyakov, Z.V. Pobedennaya, I.V. Kuksgausen, I. Karaman, Orientation dependence of twinning in single crystalline CoCrFeMnNi high-entropy alloy, Mater. Sci. Eng.: A 705 (2017) 176–181, https://doi.org/10.1016/j.msea.2017.08.065.